

Distinct Patterns of Histone Methylation and Acetylation in Human Interphase Nuclei

M. SKALNÍKOVÁ¹, E. BÁRTOVÁ², V. ULMAN¹, P. MATULA¹, D. SVOBODA¹,
A. HARNIČAROVÁ², M. KOZUBEK¹, S. KOZUBEK²

¹Centre for Biomedical Image Analysis, Masaryk University, Brno and ²Institute of Biophysics, Academy of Sciences of the Czech Republic, Brno, Czech Republic

Received September 20, 2006

Accepted January 11, 2007

On-line available February 8, 2007

Summary

To study 3D nuclear distributions of epigenetic histone modifications such as H3(K9) acetylation, H3(K4) dimethylation, H3(K9) dimethylation, and H3(K27) trimethylation, and of histone methyltransferase Suv39H1, we used advanced image analysis methods, combined with Nipkow disk confocal microscopy. Total fluorescence intensity and distributions of fluorescently labelled proteins were analyzed in formaldehyde-fixed interphase nuclei. Our data showed reduced fluorescent signals of H3(K9) acetylation and H3(K4) dimethylation (di-me) at the nuclear periphery, while di-meH3(K9) was also abundant in chromatin regions closely associated with the nuclear envelope. Little overlapping (intermingling) was observed for di-meH3(K4) and H3(K27) trimethylation (tri-me), and for di-meH3(K9) and Suv39H1. The histone modifications studied were absent in the nucleolar compartment with the exception of H3(K9) dimethylation that was closely associated with perinucleolar regions which are formed by centromeres of acrocentric chromosomes. Using immunocytochemistry, no di-meH3(K4) but only dense di-meH3(K9) was found for the human acrocentric chromosomes 14 and 22. The active X chromosome was observed to be partially acetylated, while the inactive X was more condensed, located in a very peripheral part of the interphase nuclei, and lacked H3(K9) acetylation. Our results confirmed specific interphase patterns of histone modifications within the interphase nuclei as well as within their chromosome territories.

Key words

Histone methylation • Acetylation • X chromosome • Centromeres • Image analysis

Introduction

The human genome shows a certain degree of spatial organization. A radial arrangement of chromosome territories, with gene-rich chromosomes in the nuclear interior and gene-poor chromosomes near the periphery, is a well-known phenomenon of cellular biology (for review see Cremer and Cremer 2001). Such

radial distributions of chromosomes have been described in many cell types from humans and various animals (Cremer *et al.* 2001, Tanabe *et al.* 2002, Parada *et al.* 2004, Mayer *et al.* 2005). A number of studies on structural biology showed a relationship between chromatin structure and gene expression (for review see Spector 2003). Additionally, certain regularities were observed not only for genetic elements but also for

epigenetic factors, such as posttranslational modifications of N-terminal histone tails, which play an important role in the regulation of gene expression. Histone acetylation, methylation, ubiquitination and phosphorylation were also found to be responsible for the general formation of heterochromatin and euchromatin (for review see Rice and Allis 2001, Lachner *et al.* 2003). Acetylation, mediated by histone acetyltransferases (HATs), is related to active chromatin states, while histone deacetylation, mediated by histone deacetylases (HDACs), is linked to a repressive chromatin configuration. The type of chromatin is also determined by specific histone H3 methylation on different lysine (K) residues. This important epigenetic mark is mediated by activation of histone methyltransferases (HMTs), and a newly described LSD1 histone demethylase is selectively responsible for demethylation of H3 at the position of lysine 4 (Shi *et al.* 2004, for review see Martin and Zhang 2005, Bannister and Kouzarides 2005), which is associated with transcriptionally active chromatin. On the other hand, constitutive heterochromatin is characterized by e.g. H3(K9) or H4(K20) trimethylation (Lachner *et al.* 2003, Peters *et al.* 2003, Rice *et al.* 2003, Kourmouli *et al.* 2004), while H3(K27) trimethylation was described as a marker of facultative heterochromatin (Chadwick and Willard 2004, for review see Bernstein *et al.* 2002, Lachner *et al.* 2003).

Several papers have also provided information about the nuclear organization of selected types of histone modifications. Zinner *et al.* (2006) precisely described nuclear patterns of tri-me(H3K4), mono-meH4(K20), mono-meH3(K9), tri-meH3(K27), tri-meH4(K20), and tri-me H3(K9). These histone modifications were specifically organized into distinct nuclear zones that apparently did not intermingle. In addition, using a multiple methyl-lysine antibody Cremer *et al.* (2004) provided evidence of distinct histone methylation patterns among nuclei of different cell types after exit from the cell cycle. Changes in the distribution of histone acetylation and methylation were also studied after HDAC inhibition (Taddei *et al.* 2001, Gilchrist *et al.* 2004, Bártová *et al.* 2005). These experiments revealed that the nuclear periphery in particular is a very important compartment that undergoes many changes in its histone modifications when the cells are exposed to HDAC inhibitors. Several experiments were also performed to detect histone modification on the inactive X chromosome (*Xi*), which is preferentially characterized

by H3(K9) methylation (Peters *et al.* 2002) and H4(K20) monomethylation (Kohlmaier *et al.* 2004). H3(K9) methylation was observed as a very early event in the process of X inactivation (Mermoud *et al.* 2002). Chromatin immunoprecipitation analyses revealed that H3(K9) methylation is preferentially associated with promoters of inactive genes of *Xi*, while H3(K4) is a specific marker for active genes on the active human X chromosome (*Xa*). The experiments described demonstrated that the “histone code” is deeply involved in establishing facultative and constitutive heterochromatin, and euchromatin as well.

In our experiments, we have tried to provide information about nuclear patterns of selected histone modifications. Our aim was to find changes in the nuclear distribution for euchromatic and heterochromatic epigenetic marks, particularly in respect to the nuclear periphery (as documented by Gilchrist *et al.* 2004 and Bártová *et al.* 2005) or in the relationship to nucleoli. Nuclear patterns of acetylated histones were studied in order to confirm synergism between histone methylation and acetylation processes to promote transcription (for review see Rice and Allis 2001, Martens *et al.* 2005). Nuclear distribution of HMT Suv39H1 was analysed in relationship to the H3(K9) dimethylation despite the fact that catalytic methyltransferase activity of Suv39H1 was especially studied for trimethylation of H3(K9) at pericentromeric and telomeric regions (Peters *et al.* 2003, Garcia-Cao *et al.* 2004). Moreover, the exact mechanism by which Suv39H1 interacts with chromatin is poorly understood. For example, it was suggested that the HMTs complex could be developmentally regulated in such a way that the dimethylating activity prepares histones for trimethylating state, which probably propagates transcription memory (Rice and Allis 2001, Lachner *et al.* 2003). In our experiments, high-resolution confocal microscopy, combined with image analysis methods, was found to be necessary for the suggested chromatin structure studies. Here, we have demonstrated the application of a specific image-analysis approach to the complex evaluation of fluorescence intensities and histone distribution within 3D-fixed interphase nuclei. Using our analysis we confirmed the existence of only minor intermingling of different histone lysine methylation sites, as reported by Zinner *et al.* (2006). Moreover, we showed that there was only little co-localization of di-meH3(K9) and Suv39H1 histone methyltransferase.

Methods

Cell cultivation

Primary female diploid fibroblasts were kindly provided by Prof. R. van Driel, University of Amsterdam, Netherlands. Because fluorescence signals from immunostaining were well preserved in human small lung carcinoma A549 cells (ATTC) after DNA-FISH, these cells were used for detection of selected methylation states at centromeric heterochromatin. Adherently growing cells were cultivated on coverslips in Dulbecco's modified medium (DMEM) supplemented with 10 % fetal calf serum until sub-confluence. Cells were cultured in standard conditions at 37 °C in a humidified atmosphere containing 5 % CO₂.

Immunostaining of interphase nuclei

Cells were fixed with 4 % formaldehyde in PBS for 10 min, washed twice in PBS for 5 min at room temperature (RT), permeabilized with 0.5 % Triton X-100 for 5 min (fibroblasts for 8 min) and with 0.2 % saponin for 5 min (fibroblasts for 12 min), and washed twice in PBS for 10 min. Fixed cells were then incubated for 1 h at RT in 1 % BSA dissolved in PBS. The slides were washed for 15 min in PBS, and cells were incubated with anti-acetyl-histone H3 (Lys 9) (Abcam, #ab12178), anti-dimethyl-histone H3(Lys 4) (Upstate, #07-030), anti-trimethyl-histone H3(Lys 27) (Abcam, #ab6002), anti-dimethyl-histone H3(Lys 9) (Upstate, #06-942) and anti-Suv39H1, clone MG44 (Upstate, #05-615). Each antibody was diluted 1:200 in 1 % BSA dissolved in PBS, and then incubated overnight at 4 °C. The cells were washed twice in PBS for 5 min, and incubated for 1 h with the appropriate fluorescein-conjugated secondary antibody (FITC-goat anti-rabbit IgG-whole molecule, Sigma, #F0382; FITC-anti-mouse IgG-whole molecule, Sigma, #F0257; Alexa Fluor 594-goat anti-mouse IgG₃, Molecular Probes). Immunostained cells were washed three times in PBS for 5 min, and TO-PRO-3 iodide (0.04 µg/ml, Molecular Probes) was used as counterstain. TO-PRO-3 stains both DNA and RNA, and therefore nucleoli were TO-PRO-3 positive.

For specific detection of nucleoli, in parallel with selected histone methylation and acetylation profiles, the same methodology was used. Mouse monoclonal antibody against fibrilarin in the nucleolus (Abcam, #ab12367, dilution 1:200) was applied. In these experiments, goat anti-mouse IgG₃-Alexa Fluor 594 was used as a secondary antibody.

The level of overlapping between di-meH3(K4)/tri-meH3(K27) and di-me H3(K9)/Suv39H1 was evaluated using Andor iQ software (version 1.0.1 ANDOR Technology, South Windsor, CT).

Fluorescence in situ hybridization applied after immunostaining (Immuno-FISH)

After image acquisition of immunostained nuclei (coordinates of the cell nuclei on microscopic slides were stored to the computer memory) the specimens were washed twice for 10 min in PBS and additional fixation in 4 % formaldehyde in PBS was applied for 10 min. The cells were washed in PBS three times for 5 min, permeabilized for 10 min in 0.1 N HCl, rinsed in 0.1 M Tris-HCl (pH 7.8) for 5 min, permeabilized in 0.2 % saponin in PBS and washed in 0.2 % Triton X-100 in PBS for 5 min. The slides were equilibrated in 20 % glycerol in PBS for 20 min. The target DNA was denatured in 50 % formamide in 2 × SSC for 15 min at 75 °C. The DNA probe for the X chromosome was denatured at 70 °C for 5 min and pre-annealed at 37 °C for 20 min, according to the manufacturer's instructions (ChromoTrax, Frederick Innovative Technology Center, MD; Cambio, UK). The conditions for hybridization and post-hybridization washing were selected according to the manufacturer's instructions and/or in accordance with Bártová *et al.* (2002, 2005). TO-PRO-3 iodide (0.04 µg/ml, Molecular Probes) was used again as a counterstain. After DNA-FISH, the identical cell nuclei were found on the microscopic slides according to their coordinates obtained from image acquisition of immunostained nuclei, as it was described above.

It is well known, that Immuno-FISH is a technically complicated methodology due to the DNA denaturation step (applied after immunocytochemistry) that can change the cell shape and volume. Therefore, information obtained from this technique is limited; however, it is the only methodology that can provide information about the spatial relationship between the given proteins and DNA studied within the interphase nuclei.

Image acquisition

Images of immunostained cell nuclei were acquired using a confocal system consisting of an argon/krypton laser (Innova 70, Coherent, USA), equipped with an acousto-optical tuneable filter (AOTF, Brimrose, USA) for wavelength selection, and a confocal head (QLC 100, VisiTech, UK) connected to a Leica

DMRXA epifluorescence microscope (Leica, Germany) with piezo-controlled z-movement (Physik Instrumente, Germany). The scanning system was driven by FISH 2.0 software (Kozubek *et al.* 1999) running on a PC. The images were captured with a fully programmable digital CoolSnap CCD camera (Photometrics, Tucson, AZ, USA). The magnification of the objective lens was $100\times$ (NA = 1.3). Forty optical sections, with an axial step of $0.2\ \mu\text{m}$, were scanned for each fluorochrome. Approximately 50 cells were used for our analyses.

Image processing

Since the aim of the experiment was to observe many single nuclei, we extracted each nucleus into a separate image with minimal additional space around it, using our in-house developed tool called batchcrop. Because the cells were adherent to coverslips, they were not spherical. A typical 3D image size of a cell was about $21\ \mu\text{m} \times 23\ \mu\text{m}$ laterally, but only about $5\ \mu\text{m}$ in the axial direction. We therefore decided to compute radial distributions only from maximum projection images by projecting maximum intensity values along the z-axis, resulting in 2D images. Maximum projections (so-called MP images) were computed for each 3D image of a single nucleus. The relation of 2D radial distributions computed from MP images and 3D radial distributions computed from 3D data is shown in the Image analysis section.

A binary mask image assigned to each MP nucleus image was computed by the Chan-Vese segmentation algorithm (Chan and Vese 2001) or by semi-automatic software (Kašik 2005), where needed. The purpose of the mask image was to determine which image element (pixel) is part of the nucleus and which one belongs to the image background. This information is necessary for further image analysis steps, especially for calculating signals only within the nuclear area, and for dividing the area into concentric shells.

MP images of immunostained cell nuclei were pre-processed using top-hat filtering (Soille 1999) to suppress low-frequency information. Using this filter, relevant intensity peaks corresponding to histone patterns were preserved in histone images. The structuring element (the parameter of top-hat filtering) was a disc with a diameter of 5 pixels.

Image analysis, computation of relative radial distance

We focused on the characteristic radial distributions of histone modifications within a cell

nucleus. We attempted to describe the spread of a given histone modification according to the method originally suggested by Cremer *et al.* (2001) and further developed by Cremer *et al.* (2004). Their idea for the computation of radial distributions in concentric shells was applied to our MP images.

There are two possible ways of evaluate radial distribution. In the first one, the geometrical center of the nucleus is used as a reference point (Cremer *et al.* 2004). This approach, however, depends crucially on determining the correct position of this center. In this work we decided to use another method that uses the nuclear boundary as the reference. The smallest ellipse was circumscribed around the binary mask of the whole nucleus. This ellipse was divided into N concentric ellipses, which equally (with respect to the radius) divided the nucleus area into N shells. We labeled the innermost shell as S_0 , the innermost but one as S_1 , etc. The largest one was S_{N-1} . Only pixels in the binary mask of the nucleus were taken into account in the shells. We summed up all the scattered signals in each shell, which is, due to top-hat filtering, proportional to the amount of a given histone modification in the shell:

$$P_1(i) = \frac{\sum_{j \in S_i} I(j)}{\sum_{k=0}^{N-1} \sum_{j \in S_k} I(j)}, \quad (1)$$

where $I(j)$ denotes the intensity value in the filtered image at pixel x . The denominator corresponds to the overall sum of intensities of a given histone modification within the whole nucleus, given by its binary mask. The function $P_1(i)$ expresses the radial distribution of the given histone modification in the MP images.

To determine the difference from a uniform spread radial distribution, we defined a function $P_2(i)$, which is defined as:

$$P_2(i) = \frac{A_i}{\sum_{k=0}^{N-1} A_k}, \quad (2)$$

where A_0, A_1, \dots, A_{N-1} are areas of shells S_0, S_1, \dots, S_{N-1} in pixels. Note that the equation is the same as (1) if the intensities of all pixels were set to one. This function expresses the uniform radial distribution of a signal in the cell nucleus.

We combined the probabilities computed from

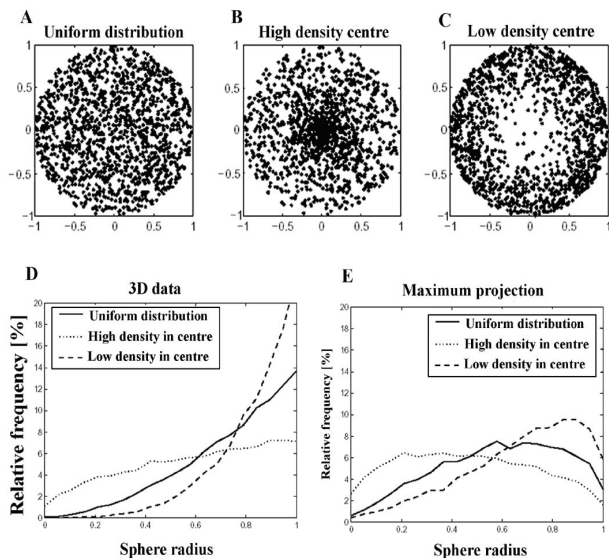


Fig. 1. Comparison of radial distributions for 3D and projected data. 10,000 points were generated in a unit sphere. Three distributions were simulated (only points with a z-coordinate close to zero are displayed): (A) uniform distribution, (B) high density in the center, low density at the periphery, and (C) high density at the periphery, low density in the center. Corresponding relative frequencies of point-to-origin distances are presented: (D) for spatial distances (no projection), (E) for distances computed after projection of points to the xy-plane.

all available data (P_1 , P_2 separately) and calculated mean values and standard deviations. By comparing such data (P_1 and P_2 functions) radial distributions with higher or lower density can be observed. To test the statistical significance of the differences in measured distributions, the Kolmogorov-Smirnov (K-S) test was applied.

We performed several simulations of radial distributions computed from MP images and 3D data. We generated three 3D point-sets of 10 000 points inside a sphere with a unit radius with the center in the origin (Fig. 1). In the first one, the points were generated with uniform distribution (Fig. 1A). In the other point-sets, the probability of being in the center was increased (Fig. 1B) or decreased (Fig. 1C). Relative frequencies of the point-to-origin distances were computed for all point-sets. The results are presented in Figure 1D.

In another simulation, the point-to-origin distances were computed for the same points projected into the xy-plane (the z-coordinate was simply omitted). The goal was to simulate the behavior of the radial distributions for MP images (Fig. 1E). Although the shape of both types of distribution functions differs for the 3D and MP cases, changes from the uniform distribution curve indicate higher or lower radial density in the data.

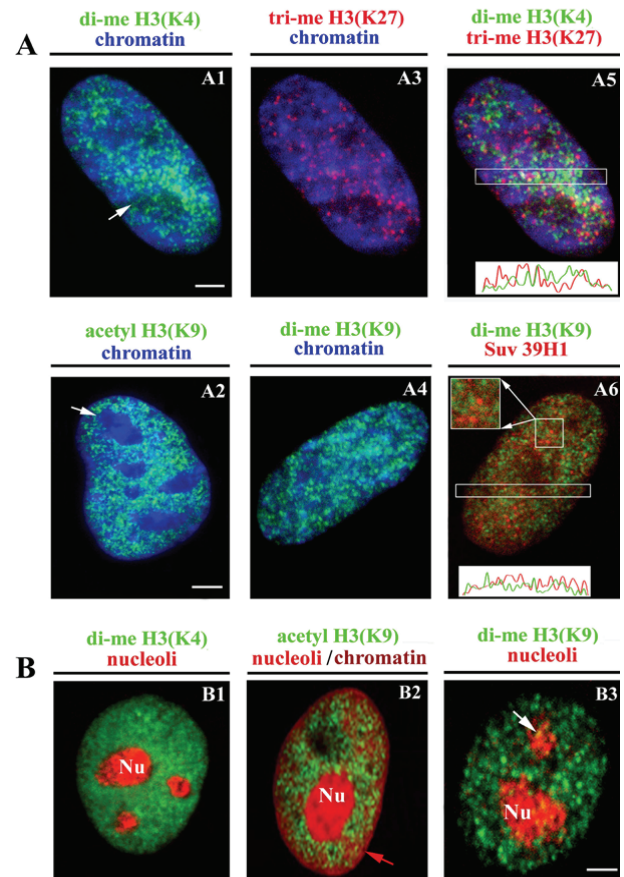


Fig. 2. Nuclear patterns for selected histone H3 modifications are shown in human primary fibroblasts. Maximum projection images from 40 optical sections are shown for: (A1) di-meH3(K4) (green); (A2) H3(K9) acetylation (green); (A3) tri-meH3(K27) (red); (A4) di-meH3(K9) (green); (A5) di-meH3(K4) (green) analysed in parallel with tri-meH3(K27) (red) and (A6) di-meH3(K9) (green) studied in parallel with the nuclear pattern of HMT Suv39H1 (red). The degree of overlapping between di-meH3(K4) (green)/tri-meH3(K27) (red) and di-meH3(K9) (green)/Suv39H1 (red) was analysed in selected regions (white rectangles in A5 and A6) and results are shown in the bottom parts of both panels A5 and A6. TO-PRO-3 (blue) was used as a counterstain in all panels shown in this section, except panel A6. Arrows in A1 and A2 indicate the absence of di-meH3(K4) and H3(K9) acetylation, respectively, in nucleolar regions. (B1) The relationship of H3(K4) dimethylation (green) to nucleoli (red); (B2) H3(K9) acetylation (green) and nucleoli (red); (B3) H3(K9) dimethylation (green) and nucleoli (red) visualised using antibody against fibrilarin (see Methods). Nu indicates nucleolus. Red arrow in B2 shows an absence of H3(K9) acetylation at nuclear periphery, white arrow in B3 shows that di-meH3(K9) densely occupies perinucleolar compartment. Bars shown in all panels represent 1 μ m.

Results

Distinct histone modification patterns were observed within interphase nuclei of human primary fibroblasts

Nuclear distributions of histone H3(K9) acetylation, di-meH3(K4), di-meH3(K9), tri-meH3(K27) and HMT Suv39H1 were studied in human primary

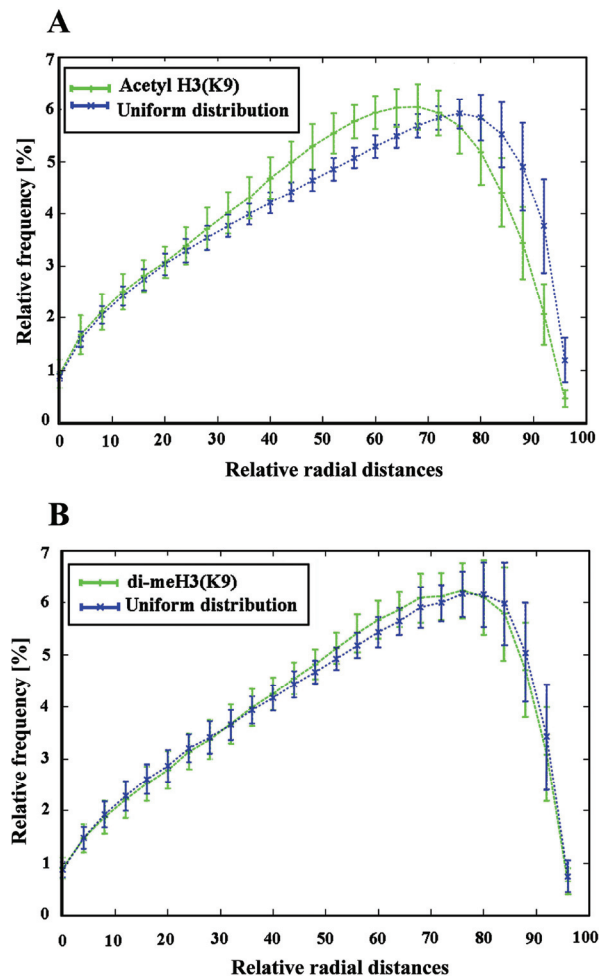


Fig. 3. Radial distribution of (A) histone H3(K9) acetylation (green) and (B) H3(K9) di-methylation (green) within interphase nuclei (blue), compared to the uniform radial distribution. Green curves correspond to the function P_1 (Eq. 1). Blue curves correspond to the function P_2 (Eq. 2). Bars (blue, green) in both figures represent standard error bars. Analysis was performed in 3D-fixed interphase nuclei; in maximum projection of images obtained from 40 confocal sections that were scanned with an axial step $0.2 \mu\text{m}$. See Methods for description in detail.

fibroblasts, using indirect fluorescence immunocytochemistry combined with high-resolution Nipkow-disk confocal microscopy. Reduced levels of di-meH3(K4) and H3(K9) acetylation at the nuclear periphery are documented in Fig. 2A1, 2A2, 2B2 and in Fig. 3A. The hypothesis of uniform distribution of H3(K9) acetylation was rejected using the K-S test on our data. On the other hand, H3(K9) dimethylation was uniformly distributed within interphase nuclei of human primary fibroblasts (Fig. 2A4), including the nuclear periphery, as documented by our analyses of interphase nuclei (Fig. 3B). Studying di-meH3(K4) (Fig. 2A1) in parallel with tri-meH3(K27) (Fig. 2A3), using dual color immunocytochemistry, we observed very little overlapping (see yellow signals and quantitative evaluation in Fig. 2A5). Similar

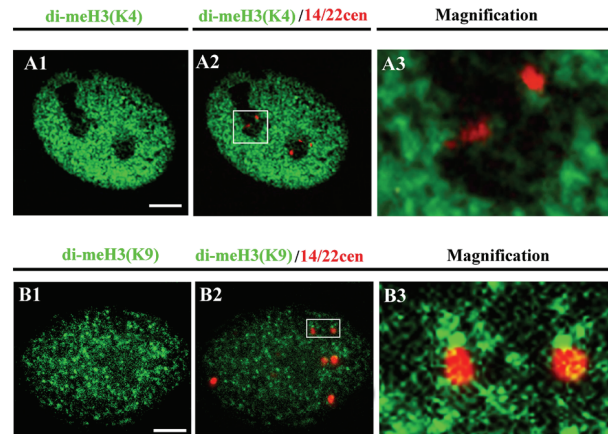


Fig. 4. H3(K4) and H3(K9) dimethylation of human alpha-satellite regions of chromosomes 14 and 22 in nuclei of human small lung carcinoma A549 cells. (A1) H3(K4) dimethylation pattern (green). (A2) The centromeres studied (red), visualized by FISH after acquisition of images of immunostained nuclei, were negative for H3(K4) di-methylation. Both figures A1 and A2 are the maximal projections of 40 confocal sections. (A3) Magnification ($7\times$) of H3(K4) dimethylated regions and centromeres selected by the square in Fig. 4A2. This image shows lack of di-meH3(K4) at human centromeric heterochromatin. (B1) H3(K9) dimethylation pattern (green). (B2) Presence of H3(K9) di-methylation at alpha-satellite sequences of human chromosomes 14 and 22 was observed. (B3) Magnification ($7\times$) of H3(K9) dimethylated centromeric regions selected by the square in Fig. 4B2. In panel 4B2, we selected only the plane, where the centromeres were located and their methylation state was distinguishable. The same plane of the identical cell, but only immunostained, is shown in Fig. 4B1. Bars represent $1 \mu\text{m}$.

observation was done for di-meH3(K9) and Suv39H1 (Fig. 2A6 and quantitative evaluation in the bottom part of Fig. 2A6). In all cases tested, the nucleoli were partially distinguishable after TO-PRO-3 staining that binds to both DNA and RNAs. Therefore, we applied additional immunostaining using antibody against fibrilarin, which confirmed the absence of di-meH3(K4) and H3(K9) acetylation at nucleolar regions (shown in Fig. 2A1, 2A2 and 2B1, 2B2). The presence of H3(K9) dimethylation at perinucleolar areas, documented in Fig. 2B3, is probably related to the fact that H3(K9) dimethylation is abundant at the centromeric regions (summarized by Lachner *et al.* 2003), which is also significant for the centromeres of the acrocentric chromosomes surrounding the nucleoli (Fig. 4, section B).

Epigenetic modifications of histones studied in centromeres of human acrocentric chromosomes 14 and 22 and in territories of the X chromosome in females

The immuno-FISH technique enabled us to study H3(K4) and H3(K9) dimethylation in the centromeric heterochromatin of human acrocentric

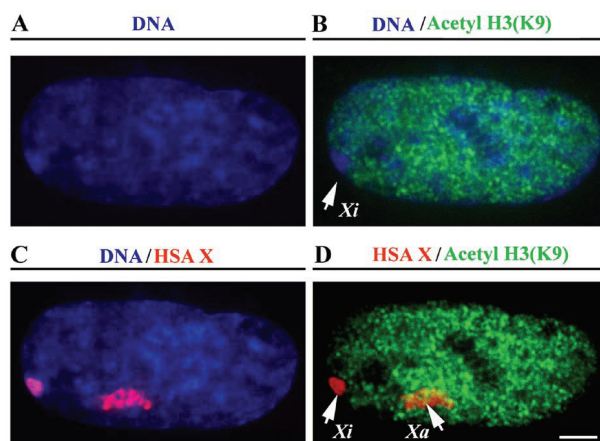


Fig. 5. H3(K9) acetylation pattern studied in both human X chromosomes from female primary fibroblasts. (A) TO-PRO-3 stained interphase nucleus (blue). (B) H3(K9) acetylation pattern (green) in the nucleus of a human primary fibroblast (blue). The inactive X (Xi) was densely stained by TO-PRO-3 (blue). (C) FISH detection of human X chromosomes (red) in the same nucleus (blue) as shown in panels A and B. The same nucleus on the microscope slide was found by its coordinates written to the computer memory. (D) Overlay of H3(K9) acetylation (green) and X chromosomes (red) showed the absence of H3(K9) acetylation on Xi and acetylation of the active X (Xa), which was additionally surrounded by highly acetylated chromatin. Bar indicates 1 μ m.

chromosomes 14 and 22 (Fig. 4). We found that the centromeres of chromosomes 14 and 22 lacked H3(K4) dimethylation (Fig. 4A3, magnification) while they were rich in H3(K9) dimethylation (Fig. 4B3, magnification). These experiments showed that not only chromatin immunoprecipitation but also immuno-FISH experiments could reveal the histone modification profiles of selected genetic regions such as centromeres.

Our immunocytochemical experiments, combined with the DNA-FISH technique and Nipkow disc confocal microscopy, further showed that the transcriptionally active (more decondensed) X chromosome (Xa) is partially H3(K9) acetylated (surrounded by highly acetylated chromatin) while Xi is very condensed, intensely stained by TO-PRO-3, located on the very periphery of the interphase nuclei, and lacks H3(K9) acetylation (see Fig. 5A-D).

Discussion

Covalent histone tail modifications, including methylation and acetylation, are important biochemical states of chromatin (Rice and Allis 2001, Mermoud *et al.* 2002, Peters *et al.* 2002). Euchromatic regions are mainly characterized by histone H3(K4) methylation and DNA hypomethylation (Noma *et al.* 2001, Bernstein *et al.*

2002, Lachner and Jenuwein 2002). On the other hand, methylation at lysine 9 residues of histone H3 is highly specific for heterochromatic regions, and is a recognition signal for binding of heterochromatic protein HP1 (Jenuwein and Allis 2001, Noma *et al.* 2001, Rice and Allis 2001, Cheutin *et al.* 2003). In addition, methylated H3(K9), H3(K27) and H4(K20) are markers for transcriptionally silent chromatin (Peters *et al.* 2003). Distinct histone methylation patterns can be observed at the locus-specific (Litt *et al.* 2001, Bernstein *et al.* 2002, Nguyen *et al.* 2002) or chromatin type-specific level (Boggs *et al.* 2002, Peters *et al.* 2002). Moreover, the degree of methylation (mono-, di-, tri-, α -4x-) determines the type of chromatin (Peters *et al.* 2002, Boggs *et al.* 2002).

Our experiments provide information on nuclear patterns of histone H3(K4) and H3(K9) dimethylation, H3(K27) trimethylation, and H3(K9) acetylation, and on the nuclear distribution of HMT Suv39H1. Our data are in good agreement with experiments published by Cremer *et al.* (2004) and Zinner *et al.* (2006), who showed that methylation patterns are well organized within interphase nuclei, and form specific zones with little apparent intermingling. In our experiments, little overlapping was observed for di-meH3(K4)/tri-meH3(K27) and for di-meH3(K9) and Suv39H1 (Fig. 2, section A). Our data imply that the enzyme Suv39H1, responsible for H3(K9) methylation, is a dynamic nuclear component that after catalysis of histone methylation probably relocates to different nuclear regions. In agreement with Bártová *et al.* (2005), we also documented (Fig. 3) that specific methylation and acetylation patterns can be observed at the nuclear periphery, which seems to be a very important nuclear compartment undergoing changes in the histone code modifications in dependence on different cellular processes.

In our further experiments we have analyzed the H3(K4) and H3(K9) dimethylation patterns of centromeres of human chromosomes 14 and 22. As expected, selected centromeres were H3(K9) dimethylated, and the absence of di-meH3(K4) was found. These experiments are in a good agreement with those of Lachner *et al.* (2003), Rice and Allis (2001) or Martens *et al.* (2005). Our analyses additionally documented the absence of H3(K9) acetylation and H3(K4) dimethylation at perinucleolar regions, while H3(K9) dimethylation tightly associated with this perinucleolar compartment. This is in good agreement with the data summarized earlier by Lachner *et al.*

(2003), showing that centromeric heterochromatin is abundant in H3(K9) dimethylation. Our experiments documented that such an epigenetic profile is also related to the centromeres of acrocentric chromosomes, which form the nucleoli.

Inactivation of one of the X chromosomes in females is an important phenomenon from the point of view of histone modifications (Boggs *et al.* 2002, Mermoud *et al.* 2002, Peters *et al.* 2002). In our experiments we observed that X chromosomes of human primary fibroblasts can be specifically epigenetically modified (see Fig. 5 A-D). We have observed the absence of H3(K9) acetylation in Xi, while the active X chromosome was partially acetylated and surrounded by a densely anti-acetyl H3(K9)-stained region.

Taken together, our results show the existence of specific patterns of histone modifications, which were revealed by analyses of whole fluorescence profiles within 3D-fixed interphase nuclei. Our data in Figure 3 provided information about the spatial organization of the methylated and acetylated histones studied. Application of our methodology, for analysis of whole epigenetic profiles within 3D-fixed interphase nuclei, represents an advanced technology that provides information about spatial organization of chromatin and its specific histone modifications. On the other hand, analysis of individual

confocal section can also provide valuable information about e.g. epigenetic profiles of a given genetic element. Such an example is shown in Figure 4B (see the legend to this figure). In our experiments, we also demonstrated by simultaneous visualization of different histone modifications, and by using anti-Suv39H1, that the epigenetic patterns studied did not noticeably intermingle. Selected types of histone methylation and acetylation, and Suv39H1 HMT, preferentially occupied distinct nuclear regions, which was also partially documented by our observation of specific epigenetic profiles at centromeric heterochromatin and at both chromosomes X. The main effort of our experiments was to contribute to the topological studies on interphase chromatin, which seems to be non-randomly organized; this was also confirmed for histone modification patterns of interphase nuclei.

Acknowledgements

This work was supported by Grant Agency of the Czech Republic, grants 202/03/D033 and 204/06/0978 and by Ministry of Education of the Czech Republic, grants MSM0021622419 and LC535. We thank Dr. A. Sumner from North Berwick, East Lothian, UK for the English revision.

References

- BANNISTER AJ, KOUZARIDES T: Reversing histone methylation. *Nature* **436**: 1103-1106, 2005.
- BÁRTOVÁ E, KOZUBEK S, JIRSOVÁ P, KOZUBEK M, GAJOVÁ H, LUKÁŠOVÁ E, SKALNÍKOVÁ M, GAŇOVÁ A, KOUTNÁ I, HAUSMANN M: Nuclear structure and gene activity in human differentiated cells. *J Struct Biol* **139**: 76-89, 2002.
- BÁRTOVÁ E, PACHERNÍK J, HARNIČAROVÁ A, KOVAŘÍK A, KOVAŘÍKOVÁ M, HOFMANOVÁ J, SKALNÍKOVÁ M, KOZUBEK M, KOZUBEK S: Nuclear levels and patterns of histone H3 modification and HP1 proteins after inhibition of histone deacetylases. *J Cell Sci* **118**: 5035-5046, 2005.
- BERNSTEIN BE, HUMPHREY EL, ERLICH RL, SCHNEIDER R, BOUMAN P, LIU JS, KOUZARIDES T, SCHREIBER SL: Methylation of histone H3 Lys 4 in coding regions of active genes. *Proc Natl Acad Sci USA* **99**: 8695-8700, 2002.
- BOGGS BA, CHEUNG P, HEARD E, SPECTOR DL, CHINAULT AC, ALLIS CD: Differentially methylated forms of histone H3 show unique association patterns with inactive human X chromosomes. *Nat Genet* **30**: 73-76, 2002.
- CHAN TF, VESE LA: Active contours without edges. *IEEE Trans on Image Process* **10**: 266-277, 2001.
- CHADWICK BP, WILLARD HF: Multiple spatially distinct types of facultative heterochromatin on the human inactive X chromosome. *Proc Natl Acad Sci USA* **101**: 17450-17455, 2004.
- CHEUTIN T, MCNAIRN AJ, JENUWEIN T, GILBERT DM, SINGH PB, MISTELI T: Maintenance of stable heterochromatin domains by dynamic HP1 binding. *Science* **299**: 721-725, 2003.
- CREMER T, CREMER C: Chromosome territories, nuclear architecture and gene regulation in mammalian cells. *Nat Rev Genet* **2**: 292-301, 2001.

- CREMER M, VON HASE J, VOLM T, BRERO A, KRETH G, WALTER J, FISCHER C, SOLOVEI I, CREMER C, CREMER T: Non-random radial higher-order chromatin arrangements in nuclei of diploid human cells. *Chromosome Res* **9**: 541-567, 2001.
- CREMER M, ZINNER R, STEIN S, ALBIEZ H, WAGLER B, CREMER C, CREMER T: Three dimensional analysis of histone methylation patterns in normal and tumor cell nuclei. *Eur J Histochem* **48**: 15-28, 2004.
- GARCIA-CAO M, O'SULLIVAN R, PETERS AH, JENUWEIN T, BLASCO MA: Epigenetic regulation of telomere length in mammalian cells by the Suv39H1 and SUV39H2 histone methyltransferases. *Nat Genet* **36**: 94-99, 2004.
- GILCHRIST S, GILBERT N, PERRY P, BICKMORE WA: Nuclear organization of centromeric domains is not perturbed by inhibition of histone deacetylases. *Chromosome Res* **12**: 505-516, 2004.
- JENUWEIN T, ALLIS CD: Translating the histone code. *Science* **293**: 1074-1080, 2001.
- KAŠÍK M: Biomedical Image Segmentation Using Dual Active Contours, *Master Thesis*, Masaryk University, Brno, 2005.
- KOHLMAIER A, SAVARESE F, LACHNER M, MARTENS J, JENUWEIN T, WUTZ A: A chromosomal memory triggered by Xist regulates histone methylation in X inactivation. *PLoS Biol* **2**: E171, 2004.
- KOURMOULI N, JEPPESEN P, MAHADEVHAIHAH S, BURGOYNE P, WU R, GILBERT DM, BONGIORNI S, PRANTERA G, FANTI L, PIMPINELLI S, SHI W, FUNDELE R, SINGH PB: Heterochromatin and trimethylated lysine 20 of histone H4 in animals. *J Cell Sci* **117**: 2491-2501, 2004.
- KOZUBEK M, KOZUBEK S, LUKÁŠOVÁ E, MAREČKOVÁ A, BÁRTOVÁ E, SKALNÍKOVÁ M, JERGOVÁ A: High-resolution cytometry of FISH dots in interphase cell nuclei. *Cytometry* **36**: 279-293, 1999.
- LACHNER M, JENUWEIN T: The many faces of histone lysine methylation. *Curr Opin Cell Biol* **14**: 286-298, 2002.
- LACHNER M, O'SULLIVAN RJ, JENUWEIN T: An epigenetic road map for histone lysine methylation. *J Cell Sci* **116**: 2117-2124, 2003.
- LITT MD, SIMPSON M, GASZNER M, ALLIS CD, FELSENFELD G: Correlation between histone lysine methylation and developmental changes at the chicken beta-globin locus. *Science* **293**: 2453-2455, 2001.
- MARTENS JHA, O'SULLIVAN, RJ, BRAUNSCHWEIG U, OPRAVIL S, RADOLF M, STEINLEIN P, JENUWEIN T: The profile of repeat-associated histone lysine methylation states in the mouse epigenome. *EMBO J* **24**: 800-812, 2005.
- MARTIN C, ZHANG Y: The diverse function of histone lysine methylation. *Nat Rev Mol Cell Biol* **6**: 838-849, 2005.
- MAYER R, BRERO A, VON HASE J, SCHROEDER T, CREMER T, DIETZEL S: Common themes and cell type specific variations of higher order chromatin arrangements in the mouse. *BMC Cell Biol* **6**: 44, 2005.
- MERMOUD JE, POPOVA B, PETERS AH, JENUWEIN T, BROCKDORFF N: Histone H3 lysine 9 methylation occurs rapidly at the onset of random X chromosome inactivation. *Curr Biol* **12**: 247-251, 2002.
- NGUYEN CT, WEISENBERGER DJ, VELICESCU M, GONZALES FA, LIN JC, LIANG G, JONES PA: Histone H3-lysine 9 methylation is associated with aberrant gene silencing in cancer cells and is rapidly reversed by 5-aza-2'-deoxycytidine. *Cancer Res* **62**: 6456-6461, 2002.
- NOMA K, ALLIS CD, GREWAL SI: Transitions in distinct histone H3 methylation patterns at the heterochromatin domain boundaries. *Science* **293**: 1150-1155, 2001.
- PARADA LA, SOTIRIOU S, MISTELI T: Spatial genome organization. *Exp Cell Res* **296**: 64-70, 2004.
- PETERS AH, MERMOUD JE, O'CARROLL D, PAGANI M, SCHWEIZER D, BROCKDORFF N, JENUWEIN T: Histone H3 lysine 9 methylation is an epigenetic imprint of facultative heterochromatin. *Nat Genet* **30**: 77-80, 2002.
- PETERS AH, KUBICEK S, MECHTLER K, O'SULLIVAN RJ, DERIJCK AA, PEREZ-BURGOS L, KOHLMAIER A, OPRAVIL S, TACHIBANA M, SHINKAI Y, MARTENS JH, JENUWEIN T: Partitioning and plasticity of repressive histone methylation states in mammalian chromatin. *Mol Cell* **12**: 1577-1589, 2003.
- RICE JC, ALLIS CD: Histone methylation versus histone acetylation: new insights into epigenetic regulation. *Curr Opin Cell Biol* **13**: 263-273, 2001.
- RICE JC, BRIGGS SD, UEBERHEIDE B, BARBER CM, SHABANOWITZ J, HUNT DF, SHINKAI Y, ALLIS CD: Histone methyltransferases direct different degrees of methylation to define distinct chromatin domains. *Mol Cell* **12**: 1591-1598, 2003.

-
- SHI Y, LAN F, MATSON C, MULLIGAN P, WHETSTINE JR, COLE PA, CASERO RA, SHI Y: Histone demethylation mediated by the nuclear amine oxidase homolog LSD1. *Cell* **119**: 941-953, 2004.
- SOILLE P: *Morphological Image Analysis. Principles and Applications*. Springer, Berlin, 1999.
- SPECTOR DL: The dynamics of chromosome organization and gene regulation. *Annu Rev Biochem* **72**: 573-608, 2003.
- TADDEI A, MAISON C, ROCHE D, ALMOUZNI G: Reversible disruption of pericentric heterochromatin and centromere function by inhibiting deacetylases. *Nat Cell Biol* **3**: 114-120, 2001.
- TANABE H, MÜLLER S, NEUSSER M, VON HASE J, CALCAGNO E, CREMER M, SOLOVEI I, CREMER C, CREMER T: Evolutionary conservation of chromosome territory arrangements in cell nuclei from higher primates. *Proc Natl Acad Sci USA* **99**: 4424-4429, 2002.
- ZINNER R, ALBIEZ H, WALTER J, PETERS AH, CREMER T, CREMER M: Histone lysine methylation patterns in human cell types are arranged in distinct three-dimensional nuclear zones. *Histochem Cell Biol* **125**: 3-19, 2006.
-

Corresponding author

E. Bártová, Institute of Biophysics, Academy of Sciences of the Czech Republic, Královopolská 135, 612 65 Brno, Czech Republic. Fax: +420 5 41211293. E-mail: bartova@ibp.cz